UNIVERSITY OF CALIFORNIA
RIVERSIDE

Analysis of Flows Driven by Gravity and Chemical Potential in a Microfluidic Channel

A Thesis submitted in partial satisfaction of the
requirements or the degree of

Master of science

in

Mechanical Engineering

by

Adewale A. Oluwatimehin

December 2023

Thesis Committee:

- Dr. Bhargav Rallabandi, Chairperson
- Dr. Luat T Vuong
- Dr. Hideaki Tsutsui

The Thesis of Adewale A. Oluwatimehin is approved:

_____

_____

_____

Committee Chairperson

University of California, Riverside

ACKNOWLEDGEMENTS

I give the highest honor to God for His goodness and kindness to me and for the hope of eternal life through His Son and Savior, Jesus Christ. I also must express my profound gratitude to Professor Bhargav Rallabandi for his immense support academically, morally, and financially. He patiently and brilliantly guided me through the over a year of challenging yet rewarding research in fluid mechanics. I also received great support from several top-notch faculty members, including Professor Luat T Vuong and Professor Hideaki Tsutsui, and friends in Mechanical engineering, Chemical engineering departments at UCR. I cannot forget my undergraduate training in chemical engineering at Lamar University, where I was introduced to fluid mechanics and influenced my intelligent Professors, including Dr Tracy Benson, Dr Peyton Richmond, Dr Guo Zhanhu (Now at Northumbria University, UK), and Dr. Evan K. Wujcik (Now at The University of Maine).

My esteemed colleagues, including Syed Taqi, Mark Strother, Ari Nacius, Art Olipani, Jonathan Cadiz, Lillian Rodriguez, Robert Sing and Thomas Smith, and the Management at NAVSEA Port Hueneme Division supported and encouraged me throughout my studies. Another invaluable support system has been the Deeper life Bible Church family, including Uncle Abraham Akingbemi, Kehinde Akingbemi, Paul Olabode, Pastor Michael Chiadika, and Pastor Augustine Okafor, who supported me spiritually and in other areas.

I would be remiss if I omitted my lovely and supportive family members. My parents, Victor and Margaret Oguntimehin, Siblings: Adeniyi, Tope, Faith, Adebola, Seyi, Ade. Nieces: Favour, Faithful, Flourish, and Nephews: Tobi, Wisdom, and Williams. I love you All!

ABSTRACT OF THE THESIS

Analysis of Flows Driven by Gravity and Chemical Potential
in a Microfluidic Channel

by

Adewale A. Oluwatimehin

Master of Science, Graduate Program in Mechanical Engineering
University of California, Riverside, December 2023
Dr. Bhargav Rallabandi, Chairperson

We developed a model for analyzing flows driven chemically by the joint effect of diffusioosmosis and buoyancy-driven convection in a small microfluidic channel. The dead-end channel containing fresh water is fed salty water having a higher density. We simplified and non-denationalized the Navier-Stokes equation, and s derived an expression for the horizontal velocity, $\boldsymbol{U}$ resulting in a convoluted coupled non-linear convection-diffusion 2D system. Using Taylor-dispersion arguments to support the averaging approach, we derived an expression for concentration deviation, $C'(X, Y, T)$ and simplified the 2D system into a 1D non-linear system involving only the average concentration, $\overline{C}\ (X, T)$

We obtained a numerical solution for the mean concentration, $< C > (T)$ and the time to fill the channel using the finite volume method and MATLAB. We varied the fluid property, (the ratio of density gradient flows to concentration gradient flows) for the effect of gravity with diffusioosmosis and solely diffusioosmosis and compared with

results obtained when both factors were involved. The results show that flow proceeds faster with the joint action of gravity and diffusioosmosis in uncharged systems. Furthermore, we observed much faster flows when in charged systems due to the ionic properties of the solute, which further strengthens the electrostatic interactions of the ions with the charged channel walls.

TABLE OF CONTENTS

LIST OF FIGURES

Chapter 1

Chapter 2

Chapter 3

Chapter 4

LIST OF TABLES

Chapter 4

Chapter 1. INTRODUCTION AND BACKGROUND

1.1 Microfluidics and microchannels

A system that utilizes a small amount of fluid ranging from 10 to 500 micrometers, is referred to as microfluidics. The emergence of this technology in the 1980s brought about live-changing innovations such as DNA chips, inkjet printheads, lab-on-a-chip, micro-propulsion, micro-thermal technologies, etc [1,2,3]. In the design of systems that process small quantity of fluids, microfluidics plays a vital role to meeting the demands for automation, high-throughput screening (testing multiple biological, chemical, or pharmacological samples), and multiplexing (transferring multiple signals over a single cable line) [18]. A lab-on-a-chip (LOC) device performs on a miniaturized scale one or several laboratory analyses [6,10]. It integrates and automates multiple high-resolution laboratory techniques such as synthesis and analysis of chemicals or fluid testing into a system that fits on a chip [8]. At this scale, it is easier to control the movement and interaction of samples, causing reactions to be much more potent, and minimizing chemical waste. It also minimizes exposure to dangerous chemicals [10].

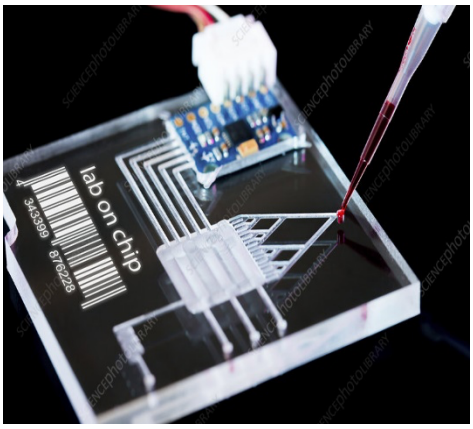

Figure 1: A microfluidic lab on a chip device. News Medical Life Sciences. https://www.news-medical-.net/life-sciences/Benefits-of-a-microfluidic-Syatem.aspx [11].

There is an increase in demand for Lab-on-a-Chip (LoC), also known as micro-total analysis system (μ-TAS). The global lab on chip business was estimated at USD 5.75 billion in 2021 and is predicted to reach around USD 15 billion by 2030 [11].

1.2 Density-driven flow in a micro-fluidic channel

Several works have been recorded of flow enabled by densities of fluids in a micro-fluidic channel including the production of polymer monolithic surfaces having a gradient of tiny opening and polymer droplet sizes from ∼0.1 to ∼0.5 μm expressed as the composition of two polymerization mixtures injected into a microfabricated chip [14]. The researchers (Kreppenhofer, K., et al.) used a micromixer connected with a Polydimethylsiloxane (PDMS) microfluidic chip to generate the gradient [14]. The process also contains a reaction chamber which serves the purpose of producing a continuous gradient film. Following polymerization inside the microfluidic chip, its inherent reversible bond open, yielding a 450μm thick film on the pore size gradient. When fluids of the

same densities were considered, and flowrates assigned for both convective mixing (20 $ml/\min$) and diffusive mixing ($\frac{0.001ml}{min}$), linear gradients were formed. Using microscopic laser-induced fluorescence (μLIF), and Scanning Electron Microscope (SEM), the emergence of density-driven 2D wedge-like was verified [14].

Concentration gradients lead to density gradients, driving convective flows. The dimensionless numbers often used to describe density-driven flows are Grashof (Gr), Reynolds (Re) and Rayleigh (Ra) numbers. The Grashof number is defined as the ratio of buoyancy forces to viscous forces [13]. The Reynolds number is the ratio of inertial forces to the viscous forces within a fluid that is subjected to relative internal movement caused by varying velocities [13]. The Rayleigh number measures the instability caused by density and temperature differences on a fluid layer at the top and bottom [13].

In their work on the impact of buoyancy on solute spreading in 2D slit and microchannel geometries, Salmon et al. (2021) [13] found that for $Ra \leq 10^3$, solutal free convection does not impact solute diffusion at all time scales. They also predicted that buoyancy would not influence molecular diffusion at higher Raleigh numbers. The group demonstrated this in an experiment involving interdiffusion between water and a 1M aqueous solution of NaCl in a microfluidic slit of height $H = 100\mu m$. Since $Ra \cong 230$ in this case, free convection is not expected to affect diffusive mixing. According to the authors, in the early stages of diffusion and advection, the longitudinal velocity of $\bar{u}_z \cong$

$25\mu m/s$ which corresponds to $5\mu m/s$ for the timescale $T = H^2/D$ that can greatly influence the advection of less mobile species dispersed in the solution [13].

1.3 Pressure-driven flow and Diffusion in a micro-fluidic channel

Due to simplicity in set-up, pressure-driven flows are often the choice for some. Moving fluids by pressure, especially in microfluidics channel of rectangular geometry poses some challenges in the distribution of analytes given that cross-sectional dimensions have parabolic velocity gradient. Molecules in the channel, regardless of the method of introduction into the device, are impacted by a position-dependent distribution in residence time. Kamholtz and Yager showed that the breadth of such a distribution is reduced by diffusion across the velocity gradient.

The T-sensor is a simple microfluidics device consisting of two input ports and one output, allowing for side-by-side flows, and operated at low Reynolds' number [16, 37].

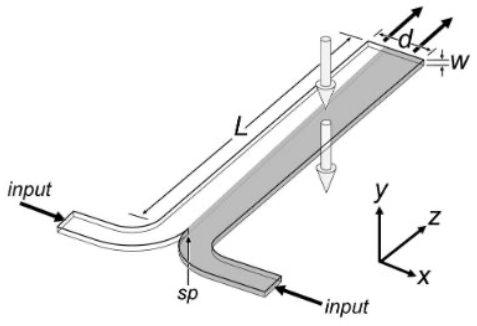

Figure 2: Conceptual rendering of the simplest form of the T-sensor. Two fluid inputs enter through channels at the bottom. In the case shown here, the fluid on the right contains a diffusible analyte (dark gray) that spreads across the d-

dimension as flow proceeds along the channel length. During operation, measurements of optical signal are made a distance downstream, L, after significant interdiffusion has occurred. Kamholtz and Yager (2001) [16]

Kamholtz and Yager [16] used T-sensor microfluidic device to show the impact of flow on diffusion due to change in position unlike pressure-driven flows which limits the usefulness of the device. T-sensor utilized low Reynolds flow conditions in microfluidic channel for chemical measurements [37]. The Peclet (Pe), is a dimensionless number used to describe the ratio between convective and diffusive transport [35]. This refers to the ratio of advection of advection of a physical quantity by the flow to the rate of diffusion of the same quantity driven by an appropriate gradient [35]. This continuum transport phenomena number is also used to describe separation and mixing.

1.4 Diffusioosmosis, Chemical potential and Charged flow.

Diffusioosmosis is a movement of fluid created the interaction between the solute and a solid surface (Huan J. Keh, 2016) [34]. This flow is often driven by an osmotic pressure gradient emanating from the concentration gradient parallel to the surface. Unlike other flows where pressure gradient enables movement, diffusioosmotic flows can occur even in the absence of pressure gradients [21,22,34]. We need not look farther than the human body where this phenomenon aids the transport of material because of concentration gradients at solid surfaces [8,21,32]. Whether in large scale industrial processes or in laboratory settings, we often encounter concentration gradients. We might make assumptions, choose certain initial conditions, and set specific boundary conditions, these factors in turn influence the concentration gradients.

Diffusiophoresis is the flow of colloidal particles in an aqueous solution of an electrolyte solution due to concentration gradient of a solute which can direct movement without the aid of an external force (Huan J. Keh, 2016) [34]. These suspended particles in solution may be in the nanometer range or possess larger diameters while the interfacial double layer region at the surface of the colloidal particle will be the order Debye length wide (typically in nanometers) [22,26,30,34]. This can be a veritable process for transferring similar small length scale particles in and out of a pore as well as preventing mixing of colloidal particles, and for several important applications (Huan J. Keh, 2016). In their work on diffusioosmosis-dispersion of colloids using Taylor dispersion analysis, Alessio et al (2022) [12] found that in the absence of mean flow, dispersion is driven by the flow created by diffusioosmotic wall slip such that spreading can be increased by increasing the diffusioosmotic mobility of the channel wall [26].

Before defining the chemical potential, we should first consider its important component: Gibbs free energy. If we have a multicomponent system, the Gibb's free energy (for pure fluid) is a function of temperature, pressure, and the number of moles of each species. The partial molar Gibb's free energy (for mixtures) is the Chemical potential which is very vital to diffusion [38,39]; it is the driving force for mass transfer; the molecules of species move from a higher chemical potential to a lower one [40]. For instance, dissolving salt in water lowers the chemical potential, making the resulting solution more stable. This is the energy released or absorbed due to changes in the particle number of a given species [38, 39].

Due to the possibility of changes in fluid properties like viscosity, it is sometimes impossible to get the optimal benefit from the intended application. The force acting on a liquid in contact with charged solid surface of the channel relies on the electrolytes in the solution, roughness, charge, and hydrophilicity [34]. Having a charged surface creates another layer known as electrical double layer (EDL) around the channel wall [34]. Consequently, at locations near the wall, ionic presence is far greater than at the center. The movement of fluid through the channel with more charges would be easily controlled. The impact of such flows can be analyzed using the physical properties of the system in consideration. Diffusioosmosis of an electrolyte solution occurs due electroosmosis, that is, the induced macroscopic electric field that is generated because tangential diffusion and convection fluxes of the two electrolyte ions are unequal [34]. This phenomenon occurs in conjunction with chemiosmosis, a condition describing the tangential gradient of the excess pressure inside the electric double layer. (Huan J. Keh, 2016) [34].

In this thesis, we develop a model for the chemically driven flow in a small microchannel caused by the combination of diffusioosmosis and buoyancy-driven convection. Our development follows that of Alessio et al [12] closely, and we will use the ideas of averaging to gain insight into the fluid flow and chemical transport.

Chapter 2. PROBLEM SET UP AND THEORY

In this chapter, we develop a modeling framework to describe the chemically driven flow in a channel due to a combination of diffusioosmotic slip and buoyancy. Using ideas of dispersion developed in Alessio et al. (2022) [12]. We reduce the coupled system governing fluid and chemical transport into a single one-dimensional diffusion-like equation for transport.

2.1 Problem setup

We consider a microfluidic channel represented by a 2D rectangular structure whose height is $2h$ and length l, where h is much smaller than l(See Fig. 2.1). The channel is filled with liquid containing dissolved salt. The concentration of solute is $c(x,t)$. Gradients of solute concentration drive flow over velocity V, due to a combination of (i) buoyancy forces and (ii) diffusio-osmotic slip at the walls due to interactions of the solute with the surfaces of the wall. The solute is transported through the channel because of molecular transport and fluid flow. Using the Navier-Stokes equations, convection-diffusion equation for chemical transport, and applying the appropriate initial and boundary conditions including diffusioosmotic slip velocities at the top and bottom walls, V_s, we determine the average concentration of solute in channel. We analyze the system for both uncharged and charged wall conditions.

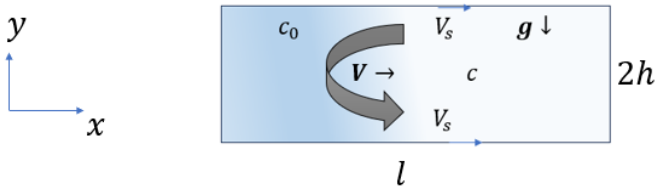

Figure 3: Schematic representing a 2D microfluidic channel of height of $2h$ and length l. Both top and bottom have a slip velocity V_s . The fluid is moving with a velocity V under the influence of gravity g, and chemical potential from the mixing concentration gradients from the denser solution(left) and the light solution (right)

2.2 Fluid Transport

We describe the fluid flow in the long microchannel using the Navier-Stokes (NS) equation. Considering the application and geometry, we simplify the equation for laminar flow having low Reynolds number. The incompressible flow is two dimensional (2D) with the vertical flow much lower than the horizontal one given the assumption that the height of the channel, h, is much smaller than the length, l . The NS equation consists of the local acceleration and convective acceleration, with mass represented by density term on the left side of the equation. On the right, we have the pressure gradient, viscous term, and body force term.

$$\rho\left(\frac{\partial \boldsymbol{V}}{\partial t} + (\boldsymbol{V}\cdot\boldsymbol{\nabla})\mathbf{V}\right) = -\boldsymbol{\nabla}p + \mu\cdot\boldsymbol{\nabla}^2\boldsymbol{V} + \rho\boldsymbol{g}\,.$$

Here, ρ and μ represent the fluid density and viscosity.

We are interested in small channels, where fluid inertia is negligible due to small Reynolds number ($\frac{\rho V h}{\mu}$ is small). An estimate for a typical flow scenario is H ~ 100 microns, V ~ 10 microns/sec, $\mu = 10^{-3}\ Pa\ s$, $\rho = 1000\ kg/m^3$.

Implementing the assumptions for negligible local acceleration of fluid in the microchannel, incompressibility ($\boldsymbol{\nabla \cdot V} = 0$), and that the vertical fluid flow direction opposes gravity hence the negative sign, NS equation simplifies to the Stokes equation below:

$$\boldsymbol{\nabla} p = \mu \boldsymbol{\nabla^2 V} - \rho g \, \boldsymbol{e_y} \ .$$

According to $\rho = \rho_0(1 + \gamma c)$, the density at initial time is ρ_0, and the density at certain concentration c is $\rho_0 \gamma c$ which is composed of the solutal expansion coefficient γ .

The vector notations for pressure, viscous, and gravity terms were decomposed to horizontal and vertical components, to yield,

$$\frac{\partial p}{\partial x} = \mu \left(\frac{\partial^2 V_x}{\partial x^2} + \frac{\partial^2 V_x}{\partial y^2} \right) . \qquad (1)$$

$$\frac{\partial p}{\partial y} = \mu \left(\frac{\partial^2 V_y}{\partial x^2} + \frac{\partial^2 V_y}{\partial y^2} \right) - \rho_0 (1 + \gamma c) g \, . \qquad (2)$$

Here, V_x and V_y are the horizontal and vertical velocities.

The following are the boundary conditions representing the diffusion-osmotic slip velocities at bottom and top of the channel as well as a zero net flux condition.

$$V_x(y = +h) = \frac{M \partial c}{\partial x}(y = +h) \, , \qquad (3)$$

$$V_x(y = -h) = \frac{M \partial c}{\partial x}(y = -h) \, , \qquad (4)$$

$$\int_{-h}^{h} V_x \partial y = 0 \ , \qquad (5)$$

where $\frac{M\partial c}{\partial x}$ is the diffusion-osmotic slip velocity at the top and bottom walls. M represents mobility proportionality constant that allows diffusioosmosis to occur as the fluid contacts the static channel wall. $\frac{\partial c}{\partial x}$ is the concentration gradient along the channel.

2.3 Solute Transport

We now consider the movement of solute through the channel as described by the following transient diffusion-advection equation.

$$\frac{\partial c}{\partial t} + \boldsymbol{V} \cdot \boldsymbol{\nabla c} = \mathrm{D}\boldsymbol{\nabla^2 c} \Leftrightarrow \frac{\partial c}{\partial t} + V_x \frac{\partial c}{\partial x} + V_y \frac{\partial c}{\partial y} = D\left(\frac{\partial^2 c}{\partial x^2} + \frac{\partial^2 c}{\partial y^2}\right) \qquad (6)$$

Expressed both in vectoral and in 2D Cartesian coordinates, the equation is composed of a transient term, advection terms, and diffusion terms. D is the diffusion coefficient, a proportionality constant between flux and concentration gradient.

2.4 Scaling Analysis and Theory

Since the PDEs (1 – 6) are challenging to solve even with the most sophisticated computer system, scientists and engineers often tackle such problems by expressing these equations in a simplified form to which approximate solutions can be obtained. To identify these simplifications, we first non-dimensionalize the system. We re-define each parameter represented in the equation as another term such that it is dimensionless. As a

result, the number of unknowns were reduced, causing the innate complexity to also decrease. By setting the terms to non-dimensional forms or re-writing the expressions to equal unity, we can compare each term with others using our chosen assumptions and determine which can be neglected because it would be significantly smaller than the other terms. This can bring about a drastic reduction in complexity, as a 3D non-linear PDE equation can be simplified to 1D linear form. Depending on the initial set up of the problem we are interested in solving, we can transform the PDE into an ODE.

In this work, we also employ redefine, re-write, compare, and simplify steps to reduce the difficulty level of the Navier- Stokes equation and the convection-diffusion equation derived earlier.

We use l and h as characteristics length scales in the horizontal (x) and vertical (y) directions, respectively. Using $l \gg h$, we derive an expression for pressure, p, the horizontal pressure gradient, and the vertical pressure gradient after neglecting the less predominant terms, $\frac{\partial^2 V_x}{\partial x^2}$. Thus, balancing viscous stress in the horizontal momentum equation, we obtain the pressure scale.

$$\frac{p}{l} \sim \frac{\mu {V_x}^*}{h^2} \rightarrow p \sim \frac{\mu {V_x}^* l}{h^2}$$

Similarly, we perform scaling on equation (2), and neglecting the term containing the smaller horizontal length, $\frac{\partial^2 v_y}{\partial x^2}$. So, we are left with the following equations:

$$\frac{\partial p}{\partial y} \cong -\rho_0(1+\gamma c)\,. \tag{7}$$

$$\frac{\partial p}{\partial x} \cong \mu\frac{\partial^2 V_x}{\partial y^2}\,. \tag{8}$$

Taking derivatives with respect to y on equation (7) and with respect to x on equation (8) and equating the resulting expressions, we obtain:

$$\frac{\mu\partial^3 V_x}{\partial y^3} = -\frac{\rho_0 g\gamma\partial c}{\partial x}\,. \tag{9}$$

We rescale equations (5) and (6) to obtain the expression for characteristic velocity of flow driven by density gradients, V_g,(convective flow) and the characteristic velocity of flow driven by concentration gradients, V_c. A balance between buoyancy forces and viscous forces, which can be expressed as $\frac{\mu V}{h^3} \sim \frac{\rho_0 g\gamma c^*}{l}$, identifies

$$V_g \sim \frac{\rho_0 g\gamma c^* h^3}{\mu l}\,, \tag{10}$$

where c^* is a concentration scale. The velocity scale due to diffusion-osmotic slip is

$$V_c \sim \frac{Mc^*}{l}\,. \tag{11}$$

We define non-dimensional quantities for horizontal velocity (U), height (Y), length (X), and concentration C according to:

$$U = \frac{V_x}{V_c} \Rightarrow V_x = V_c U(X,Y)\,. \tag{12}$$

$$Y = \frac{y}{h} \quad \Rightarrow \quad y = hY \ . \tag{13}$$

$$X = \frac{x}{l} \quad \Rightarrow \quad x = lX \ . \tag{14}$$

$$C = \frac{c}{c^*} \quad \Rightarrow \quad c = c^* C \ . \tag{15}$$

We note that U and C implicitly also depend on time, we then substitute equations (11) through (15) into equation (9) to obtain the following:

$$\frac{\mu V_c}{h^3} \frac{\partial^3 U}{\partial Y^3} = -\frac{\rho_0 g \gamma c^*}{l} \frac{\partial C}{\partial X} \ . \tag{16}$$

$$\frac{\partial^3 U}{\partial Y^3} = -\frac{\rho_0 g \gamma c^* h^3}{l \, \mu V_c} \frac{\partial C}{\partial X} \ . \tag{17}$$

Recalling equation (9), and simplifying equation (16), and defining

$$\Gamma = \frac{\mathrm{V_g}}{V_c} = \frac{\rho_0 g \gamma c^* h^3}{\mu M} \tag{18}$$

we obtain the simplified (approximate) equation for the dimensionless horizontal velocity.

$$\frac{\partial^3 U}{\partial Y^3} = -\Gamma \frac{\partial C}{\partial X} \, . \tag{19}$$

The non-dimensional boundary conditions obtained from equations (3), (4), and (5)

$$U(Y = 1) = \frac{\partial C}{\partial X} \, . \tag{20}$$

$$U(Y = -1) = \frac{\partial C}{\partial X} \, . \tag{21}$$

$$\int_{-1}^{1} U\,\partial Y = 0\ . \tag{22}$$

To solve the horizontal velocity, we integrate equation (19) three times to obtain an expression for U,

$$U = -\Gamma\left(\frac{\partial C}{\partial X}\frac{Y^3}{6} + d_1\frac{Y^2}{2} + d_2\,Y + d_3\right), \tag{23}$$

where $d_1\,, d_2, and\ d_3$ are integration constants.

Applying the boundary conditions and the flux condition $(20-22)$, we determined the constants of integration to be $d_1 = -\frac{3}{\Gamma}\frac{\partial C}{\partial X}\,, d_2 = -\frac{1}{6}\frac{\partial C}{\partial X}\ \,, d_3 = \frac{1}{2\Gamma}\frac{\partial C}{\partial X}$. Substituting these values into equation(22) and further simplifying yields

$$U = -\frac{\partial C}{\partial X}\left[\frac{\Gamma}{6}\,(Y^3 - Y) + \frac{1}{2}\,(1 - 3Y^2)\right]. \tag{24}$$

Now that we have obtained an approximation for the horizontal velocity, U, we will proceed to the get an expression the vertical velocity, V. Like the horizontal velocity U, $V = \frac{V_y}{V_y^*}$ is the non-dimensional vertical velocity, and $V_y^* = \frac{v_c h}{l}$ is the characteristic vertical velocity scale. We apply the continuity equation to establish a relationship between U and V,

$$\frac{\partial V}{\partial X} = -\frac{\partial U}{\partial X}.$$

We then substitute the expression in equation (24) for U , integrate with respect to Y, and apply Boundary conditions at $Y = \pm 1$ as in equations (20) through (22). The resulting expression for vertical velocity is therefore:

$$V = -\frac{\partial^2 C}{\partial X^2}\left[\frac{\Gamma}{6}\left(\frac{Y^4}{4} - \frac{Y^2}{2} + \frac{1}{4}\right) + \frac{1}{2}\left(Y - Y^3\right)\right] \qquad (25) \quad .$$

Figure (4) plots profiles of velocities [horizontal(U) and vertical (V)] across the cross-sectional coordinate, Y of the channel vs the velocities [horizontal(U) and vertical (V)]. The blue curve represents horizontal velocity, and the red curve is the vertical velocity. We observed that curve U is maximum close to $Y = 0$ the center of the channel. However, the maximum may shift up or down depending on the value of Γ.It is also worthy to note that at $Y = \pm 1$, the fluid velocity is not zero, confirming the effect of diffusioosmosis.

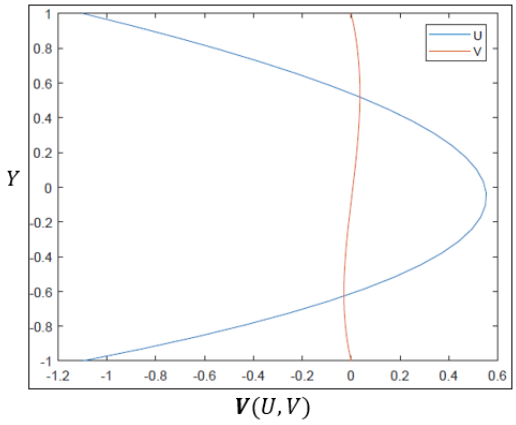

Figure 4. Velocity profile of channel cross-sectional height, Y vs velocities $\boldsymbol{V}(U,V)$. We consider the effect of gravity and diffusioosmosis for uncharged system with flow parameters, $\Gamma = 1$.

Next, we rescale each term represented in equation (6). The typical scale of each term is given below

$\frac{\partial c}{\partial t} \sim \frac{c^*}{t^*}$ Transient term (I)

$V_x \frac{\partial c}{\partial x} \sim V_c \frac{c^*}{l}$ Horizontal Advective term (II)

$V_y \frac{\partial c}{\partial y} \sim \frac{h}{l} V_c \frac{c^*}{h}$ Advective term (III)

$D \frac{\partial^2 c}{\partial x^2} \sim D \frac{c^*}{l^2}$ Horizontal Diffusive term (IV)

$D \frac{\partial^2 c}{\partial y^2} \sim D \frac{c^*}{h^2}$ Vertical Diffusive term (V)

Since $l \gg h$, that is, the dominant term with which we compare transient term are the horizontal advective term. Whereas the transient term is compared with the vertical diffusive term due to the action of gravity, and given the above vertical-horizontal length scale, it would take longer to diffuse across the length of the channel. To determine the duration of both advection and diffusio-osmosis in the channel, we linearly compare the vertical diffusive term $(D \frac{c^*}{h^2})$ and horizontal advective term $(V_c \frac{c^*}{l})$ separately with the transient term $(\frac{c^*}{t^*})$ in equation (6) . This results in advective time scale, $t_a^* = \frac{l}{v_c}$ and diffusive time scale, $t_d^* = \frac{h^2}{D}$. We represent characteristic concentration and characteristic time (which could be diffusive or advective depending on the reference for comparison) as $c^* \; and \; t^*$, respectively.

We are then non-dimensionalize equation (6) as shown below:

$$\frac{\partial C}{\partial T} + V_c \frac{t^*}{l} U \frac{\partial C}{\partial X} + \frac{h}{l} V_c \frac{c^*}{h} t^* V \frac{\partial C}{\partial Y} = \frac{D}{l^2} t^* \frac{\partial^2 C}{\partial X^2} + \frac{D}{h^2} t^* \frac{\partial^2 C}{\partial Y^2}. \quad (26)$$

Where we have defined $T = t/t^*$, $\varepsilon = \frac{h}{l}$ and $\mathcal{D} = \frac{Dl}{h^2 v_c}$

We rewrite equation (26) using ε, the geometry scaling factor (which is small), and $\mathcal{D}$, the non-dimensional diffusivity which compares to the advection across the channel, leading to

$$\frac{\partial C}{\partial T} + U \frac{\partial C}{\partial X} + V \frac{\partial C}{\partial Y} = \mathcal{D}\left(\frac{\partial^2 C}{\partial Y^2} + \varepsilon^2 \frac{\partial^2 C}{\partial X^2}\right). \quad (27)$$

Eqn. (27) describes the two-dimensional transport of solute in the channel, written in dimensionless form. Our goal is to obtain a simplified description of the average solute transport in the channel, in which the variations across the channel (along the Y axis) are averaged out. To achieve this, we first decompose the concentration in the channel $C(X, Y, T)$ as the sum of average concentrations, $\overline{C}$ and deviation from average, C'. (Alessio et al., 2022) [12]. The former refers to the cross-sectional average concentration of solute at different positions and times, and the later describes perturbation, accounting for the slight variations from the original concentration due to instabilities emanating from flow in the vector field. Mathematically, these quantities are defined according to

$$C(X,Y,T) = \overline{C}\,(X,T) + C'(X,Y,T). \qquad (28)$$

$$\overline{C}\,(X,T) = \frac{1}{2}\int_{-1}^{1} C(X,Y,T)$$

$$C'(X,Y,T) = C(X,Y,T) - \overline{C}\,(X,T)$$

We then substitute equation (28) into equation (27)

$$\frac{\partial(\overline{C}+C')}{\partial T} + \frac{\partial(U(\overline{C}+C'))}{\partial X} + \frac{\partial(V(\overline{C}+C'))}{\partial Y} = \mathcal{D}\left(\varepsilon^2 \frac{\partial^2(\overline{C}+C')}{\partial X^2} + \frac{\partial^2(\overline{C}+C')}{\partial Y^2}\right). \qquad (29)$$

Next, we take the average of (29) across the height of the channel to determine the average transport of solute, to arrive at the following:

$$\frac{\partial\overline{C}}{\partial T} + \frac{\partial}{\partial X}\left(\overline{U\overline{C}} + \overline{UC'}\right) + \overline{\frac{\partial}{\partial Y}(VC)} = \mathcal{D}\left(\varepsilon^2 \frac{\partial^2\overline{C}}{\partial X^2} + \overline{\frac{\partial^2}{\partial Y^2}\left(\overline{C}+C'\right)}\right). \qquad (30)$$

Integrating (or averaging) equation (29) with respect to Y from-1 to 1 allows for the elimination of all derivatives with respect to Y. Equation (30) then simplifies to:

$$\frac{\partial\overline{C}}{\partial T} + \frac{\partial}{\partial X}\overline{U\overline{C}} + \frac{\partial}{\partial X}\overline{UC'} = \mathcal{D}\varepsilon^2 \frac{\partial^2\overline{C}}{\partial X^2}. \qquad (31)$$

Approximation for C'

Next, we find an approximation for concentration deviation, C' by first subtracting equations (30) from equations (27).

$$\frac{\partial C'}{\partial T} + U\frac{\partial \overline{C}}{\partial X} + U\frac{\partial C'}{\partial X} + V\frac{\partial \overline{C}}{\partial Y} + V\frac{\partial C'}{\partial Y} - \frac{\partial}{\partial X}\,\overline{U\overline{C}} - \frac{\partial}{\partial X}\,\overline{UC'}$$

$$= \mathcal{D}\left(\frac{\partial^2 C'}{\partial X^2} + \frac{\partial^2 C'}{\partial Y^2}\right). \qquad (32)$$

The scale of each term in the equation is estimated and compared with other terms, with a view to determining which would be neglected while retaining the dominant terms. In addition to the length (l) being much greater than the height (h), the concentration deviation (C') is also much smaller than the average concentration ($\overline{C}$). The characteristic scales of transient and advective terms on the left side of equation (32) are approximated below:

$$\frac{\partial C\prime}{\partial T} \sim \frac{C'}{T}, \quad U\frac{\partial \overline{C}}{\partial X} \sim U\frac{\overline{C}}{l}, \; U\frac{\partial C\prime}{\partial X} \sim U\frac{C\prime}{l}, V\frac{\partial \overline{C}}{\partial Y} \sim V\frac{\overline{C}}{h}, V\frac{\partial C'}{\partial Y} \sim V\frac{C'}{h}, \; \frac{\partial}{\partial X}\,\overline{U\overline{C}} \sim U\frac{C}{l},$$

$$\frac{\partial}{\partial X}\,\overline{UC'} \sim U\frac{C'}{l}$$

Similarly, the diffusive terms on the right have the following scaling expressions:

$$\mathcal{D}\frac{\partial^2 C\prime}{\partial X^2} \sim \mathcal{D}\frac{C'}{l^2}, \quad \mathcal{D}\frac{\partial^2 C\prime}{\partial Y^2} \sim \mathcal{D}\frac{C'}{h^2}$$

Since $\mathcal{D}\frac{\partial^2 C\prime}{\partial X^2} \ll \mathcal{D}\frac{\partial^2 C\prime}{\partial Y^2}$ we neglected the X derivative, and $V\frac{\partial C'}{\partial Y} \ll U\frac{\partial \overline{C}}{\partial X}$ in congruent with the established fact that C' is much smaller than $\overline{C}$. After comparing dominant terms and neglecting sub-dominant terms, we obtain

$$\frac{\partial C'}{\partial T} + U\frac{\partial \overline{C}}{\partial X} - \frac{\partial}{\partial X}\left(\overline{U\overline{C}}\right) = \mathcal{D}\frac{\partial^2 C'}{\partial Y^2}. \tag{33}$$

Equation (33) can be simplified further by comparing the transient term with the diffusive term.

Seeking solutions for long times $T \gg h^2/\mathcal{D}$, we eliminate the transient term. Also, the advective term, $\frac{\partial}{\partial X}\left(\overline{U\overline{C}}\right)$ = 0. Therefore, the PDE with which we find an approximation for concentration deviation, C' is:

$$U\frac{\partial \overline{C}}{\partial X} \cong \mathcal{D}\frac{\partial^2 C'}{\partial Y^2} \tag{34}$$

We then substitute the expression for *U* in equation (24), using the approximation $\left(\frac{\partial C}{\partial X}\right) \cong \left(\frac{\partial \overline{C}}{\partial X}\right)$ [since $C' \ll \overline{C}$]. Rearranging, we obtain

$$\frac{\partial^2 C\prime}{\partial Y^2} \cong \frac{1}{\mathcal{D}}\left(\frac{\partial \overline{C}}{\partial X}\right)\left(\frac{\partial C}{\partial X}\right)\left[\frac{\Gamma}{6}(Y - Y^3) + \frac{1}{2}(3Y^2 - 1)\right]. \quad (35)$$

Upon integrating twice, we have

$$C' \cong \frac{1}{\boldsymbol{D}}\left(\frac{\partial \overline{C}}{\partial X}\right)^2\left[\frac{\Gamma}{6}\left(\frac{Y^3}{6} - \frac{Y^5}{20}\right) + \frac{1}{2}\left(\frac{Y^4}{4} - \frac{Y^2}{2}\right) + \mathrm{d}_1 Y + d_2\right],$$

Applying the boundary conditions: $\frac{\partial C'}{\partial Y} = 0,\ Y = \pm 1$, we obtain the value for $d_1 = -\frac{\Gamma}{24}$. Also, asserting that $\int_{-1}^{1} C'\, dY = 0$ (which is true by definition), gives the value of $d_2 = \frac{7}{120}$. Now substituting the values of $d_1\ and\ d_2$ into equation (33) we obtain an expression for C' .

$$C' \cong \frac{1}{\mathcal{D}}\left(\frac{\partial \overline{C}}{\partial X}\right)^2\left[\frac{\Gamma}{12}\left(\frac{Y^3}{3} - \frac{Y^5}{10} - \frac{Y}{2}\right) + \frac{1}{4}\left(\frac{Y^4}{2} - Y^2 + \frac{7}{30}\right)\right]. \quad (36)$$

We adopt the previous simplification that $\left(\frac{\partial C}{\partial X}\right) \cong \left(\frac{\partial \overline{C}}{\partial X}\right)$, and use Mathematica to perform integration of equation (35) from $Y = -1\ to\ Y = 1$, resulting in the following expression for $\overline{UC'}$.

$$\overline{UC'} \cong -\frac{4}{\mathcal{D}}\left(\frac{\partial \overline{C}}{\partial X}\right)^3 \frac{(27+\Gamma^2)}{2835} \quad (37)$$

Substituting equation (37) into equation (31), noting that $\overline{U\overline{C}} = \overline{U}\,\overline{C}\ and\ \overline{U} = 0$, we eliminate $\frac{\partial}{\partial X}\left(\overline{U\overline{C}}\right)$ term, finally simplifying the equation (31) to the one-dimensional transport equation

$$\frac{\partial \overline{C}}{\partial T} = \frac{\partial}{\partial X}\left[\left(\frac{4}{\mathcal{D}}\left(\frac{\partial \overline{C}}{\partial X}\right)^3 \frac{(27+\Gamma^2)}{2835}\right) + \left(\mathcal{D}\varepsilon^2 \frac{\partial \overline{C}}{\partial X}\right)\right]. \qquad (38)$$

Starting with Navier Stokes and solute transport equation, which is complicated, we simplified the equation to a 1D non-linear diffusion-like partial differential equation. The non-linear term $\left(\frac{\partial \overline{C}}{\partial X}\right)^3$ is the consequence of transport of solute by the solute generated fluid flow. The term involving Γ^2 is the effect of gravity, whereas the $\left(\frac{\partial \overline{C}}{\partial X}\right)^3$ term independent of Γ is the effect of diffusio-osmotic slip. The last term on the right is pure diffusion, which occurs even in the absence of fluid flow. While equation (38) is a significant simplification over the original coupled fluid and transport. It is still nonlinear, so it must be solved numerically (discussed in the following chapters).

2.5 Charged Transport

Often, the walls of the channel have slight net charge. If the solute is ionic (e.g., NaCl), there are electrostatic interactions of the ions with the charged wall. In this case, the mobility M_c relation is slightly modified from before. Now the slip velocity at the top and bottom walls of the channel, V_s given by (Alessio et al., 2022) [12]

$$V_s =$$

$$\frac{1}{C} M_c \frac{\partial c}{\partial x} . \qquad (39)$$

The scaled flow velocities due to gravity V_g, and concentration V_c are thus expressed as follows:

$$V_g =$$

$$\frac{\rho_0 g c^* h^3}{\mu l} . \qquad (40)$$

$$V_c = \frac{M_c c^*}{c^* l} =$$

$$\frac{M_c}{l} . \qquad (41)$$

For charged surfaces, we define gravity parameter.

$$\Gamma^c = \frac{V_g}{V_c} =$$

$$\frac{\rho_0 g c^* h^3}{\mu M_c} . \qquad (42)$$

Where Γ^c represent the ratio of gravity flow to the concentration flow for the charged case.

Substitute equation (38) into equation (24) to obtain a modified expression for charged horizontal fluid velocity, U^c.

$$U^c = -\frac{\partial C}{\partial X}\left[\frac{\Gamma^c}{6}(Y^3 - Y) + \frac{1}{2C}(1 - 3Y^2)\right]. \quad (43)$$

Recall $\mathcal{D} = \frac{Dl}{h^2 V_c}$, substitute $V_c = \frac{M_c}{l}$ to get the charged representation, $\mathcal{D}^c$.

$$\mathcal{D}^c = \frac{Dl^2}{M_c h^2}$$

Using the same procedures for deriving the expression in equation (30) and replacing U and $\mathcal{D}$ with U^c and $\mathcal{D}^c$ respectively.

$$U^c \frac{\partial \overline{C}}{\partial X} \cong \mathcal{D}^c \frac{\partial^2 C'}{\partial Y^2}. \quad (44)$$

Similarly, we obtain the charged expression for the charged C'.

$$C' \cong \frac{1}{\mathcal{D}^c}\left(\frac{\partial \overline{C}}{\partial X}\right)^2 \left[\frac{\Gamma^c}{12}\left(\frac{Y^3}{3} - \frac{Y^5}{10} - \frac{Y}{2}\right) + \frac{1}{4\overline{C}}\left(\frac{Y^4}{2} - Y^2 + \frac{7}{30}\right)\right]. \quad (45)$$

Following steps as before, we obtain the effective transport equation for the charged case

$$\frac{\partial \overline{C}}{\partial T} = \frac{\partial}{\partial X}\left[\left(\frac{4}{\mathcal{D}^c}\left(\frac{\partial \overline{C}}{\partial X}\right)^3 \frac{\left(\frac{27}{\overline{C}^2} + \Gamma^{c^2}\right)}{2835}\right) + \left(\mathcal{D}^c \varepsilon^2 \frac{\partial \overline{C}}{\partial X}\right)\right]. \quad (46)$$

The above equation is like (38) for the uncharged case, except for one term corresponding to slip.

Thus, we have reduced the non-linear coupled velocity and concentration 2D system in equation (6) to a single 1D non-linear equation involving only concentration as shown in both equation (38) for uncharged, and in equation (46) for charged walls. In the following chapters we solve these equations numerically, and present results.

Chapter 3. NUMERICAL SOLUTION METHODOLOGY

In this short chapter we outline the numerical method that we used to solve for the solute transport.

3.1 Finite Volume Method

We utilized the finite volume method to solve the non-linear equation [equation (38)]. First, we divided the channel length into n equal cells or segments. The flux, J of 'material' leaving a segment is the same entering the next cell. The average concentration lies at the midpoint of each cell, and the distance between one midpoint and the next is ΔX. Figure 3 illustrates a rectangular structure of length $l = 1$, and having $n = 5$ cells. Each cell serves as the reference point or location for determining the average concentration. The flux to the far left is $J_{0.5}$ and to the far right of the grid is $J_{5.5}$.

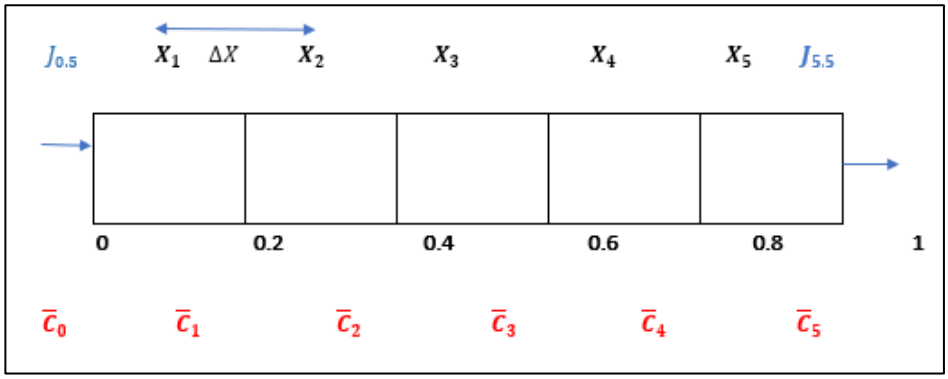

Figure 5: A schematic showing flux J in and out of solution whose average concentration $\overline{C}$ is located at the center of each grid X. The change in X direction is the distance between two midpoints of adjacent grids, ΔX. An illustration of the application of Finite volume method.

We outline the method through a list of steps.

Step 0: First, we write the transport equation in terms of a general conservation law

$$\frac{\partial \overline{C}}{\partial T} + \frac{\partial}{\partial X} J = 0 \qquad (47)$$

From the general equation for an arbitrary flux (47) , we define the flux, J as for (i) pure diffusion , (ii) uncharged wall, and (iii) charged wall cases as $-\mathcal{D}\frac{\partial \overline{C}}{\partial X}$,

$-\left(\left(\frac{4}{\mathcal{D}}\left(\frac{\partial \overline{C}}{\partial X}\right)^3 \frac{(27+\Gamma^2)}{2835}\right) + \left(\mathcal{D}\varepsilon^2 \frac{\partial \overline{C}}{\partial X}\right)\right)$ and $-\left(\left(\frac{4}{\mathcal{D}^c}\left(\frac{\partial \overline{C}}{\partial X}\right)^3 \frac{\left(\frac{27}{\overline{C}^2}+\Gamma^{c^2}\right)}{2835}\right) + \left(\mathcal{D}^c\varepsilon^2 \frac{\partial \overline{C}}{\partial X}\right)\right)$,

respectively.

Step 1: We write the finite difference approximation for flux by substituting $\left(\overline{C}_{i+1} - \overline{C}_i\right)$ for $\partial \overline{C}$, and ΔX in place of ∂X in step 0. The following are the fluxes to the right of each cell i or $J_{i+1/2}$, for all three categories mention earlier.

$$J_{i+1/2} \cong -\frac{\mathcal{D}(\overline{C}_{i+1} - \overline{C}_i)}{\Delta X} \qquad \text{(pure diffusion)}$$

$$J_{i+1/2} \cong -\left(\left(\frac{4}{\mathcal{D}}\left(\frac{\overline{C}_{i+1} - \overline{C}_i}{\Delta X}\right)^3 \frac{(27+\Gamma^2)}{2835}\right) + \left(\mathcal{D}\varepsilon^2 \frac{\overline{C}_{i+1} - \overline{C}_i}{\Delta X}\right)\right) \qquad \text{(uncharged)}$$

$$J_{i+1/2} \cong -\left(\left(\frac{4}{\mathcal{D}^c}\left(\frac{\overline{C}_{i+1} - \overline{C}_i}{\Delta X}\right)^3 \frac{\left(\frac{27}{\overline{C}^2}+\Gamma^{c^2}\right)}{2835}\right) + \left(\mathcal{D}^c\varepsilon^2 \frac{\overline{C}_{i+1} - \overline{C}_i}{\Delta X}\right)\right) \qquad \text{(Charged)}$$

Step 2: We write an equation to advance transport equation (47) in time.

$$\left(\frac{\partial \overline{C}}{\partial T}\right)_i \cong \frac{\overline{C}_i(T+\Delta T)-\overline{C}_i(T)}{\Delta T} \quad (48)$$

Where $\overline{C}_i(T+\Delta T)$ represent average concentration at next time, and $\overline{C}_i(T)$ the average concentration at current time. We then use finite differences in space to write

$$\left(\frac{\partial J}{\partial X}\right)_i \cong \frac{J_{i+\frac{1}{2}}- J_{i-\frac{1}{2}}}{\Delta X} \quad (49)$$

where $J_{i-\frac{1}{2}}$ represents fluxes at previous position.

We now substitute equations (48) and (49) into equation (47), and rearrange the resulting equation to get an expression for $\overline{C}_i(T+\Delta T)$

$$\frac{\overline{C}_i(T+\Delta T)-\overline{C}_i(T)}{\Delta T} + \frac{J_{i+\frac{1}{2}}- J_{i-\frac{1}{2}}}{\Delta X} = 0$$

$$\overline{C}_i(T+\Delta T) = \overline{C}_i(T) - \frac{\Delta T}{\Delta X}\left(J_{i+\frac{1}{2}} - J_{i-\frac{1}{2}}\right) \quad (50)$$

We started by discretizing the modified general diffusion equation and used that as guide also discretize the models (equations 38 and 46) we developed and will solve numerically. Equipped with the "computer-friendly" form for each component of our non-

linear PDE, we implemented the necessary codes using MATLAB and obtained interesting results, which we discuss in the next chapter.

Chapter 4. RESULTS AND ANALYSIS

We now consider the major result found in equation (46) and then compare for the charged case. The right-hand side comprises of the fluid properties including gravity that influences the bulk flow, and a concentration gradient term. The second term represents the pure diffusion including the channel geometry and concentration gradient. The finite volume method was implemented into MATLAB to create a model with which we can tune and modify parameters such as $\Gamma, \mathcal{D}, \text{and } \varepsilon$ to determine how the concentration in the channel changes as time progresses. The effect of gravity embedded in the Γ term is expected to influence the mixing process causing molecules to move fast or slow from a higher concentration to a lower concentration until steady state or equilibrium concentration is reached.

To show that flow can be influenced with both the action of gravity and chemical potential, we consider the follow four (4) scenarios which includes: (i) pure diffusion; (ii) gravity or bulk flow; (iii) uncharged flow with diffusioosmosis and gravity; (iv) charged flow with diffusioososis and gravity. In each case, we study the time taken for the solute concentration to reach 95 percent of the channel capacity for different parameters.

Filling of a dead-end pore: We now focus our attention on the specific situation of a dead-end pore initially filled with fresh water (figure 6 a), exposed to salty water (figure 6 b), at inlet or opened end as shown in figure 6. In figure 6 (c, d, e), we show the evolution of diffusion of salt in the channel. We then write the initial conditions:

$\overline{C}(X,\ T=0)=0$, and the boundary conditions $\overline{C}(X=0,\ T)=\ \overline{C}_0$ and boundary conditions: $\frac{\partial \overline{C}}{\partial X}(X=1,T)=0$,

We solve equation (38) ,and subsequently, equation (46) for the charged case.

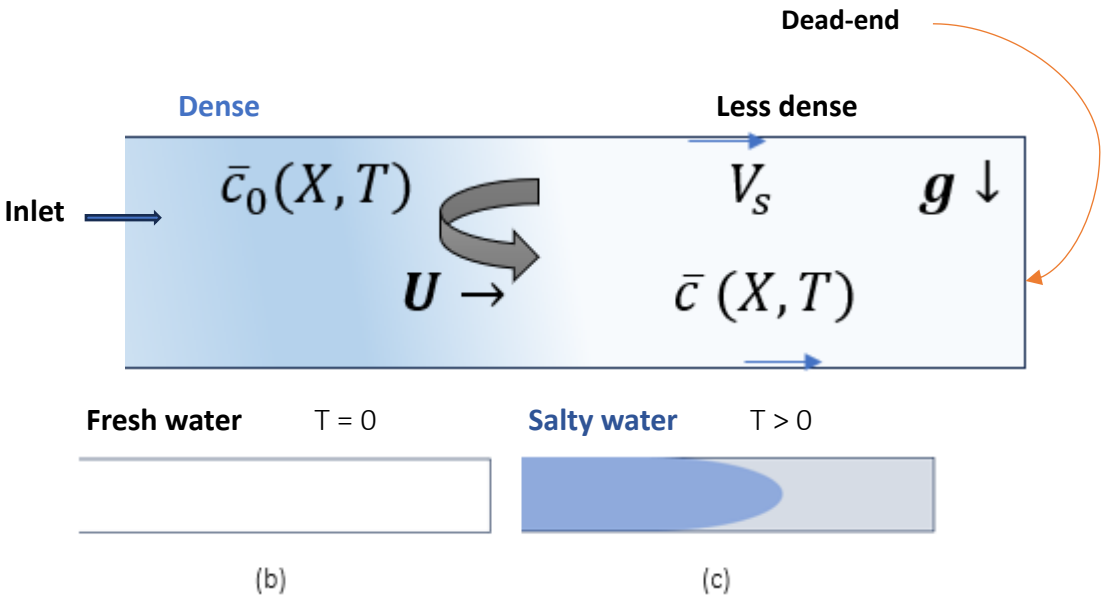

Figure 6. (a) A sketch of the dead-end microfluidic channel with an opened left end where the salty solution was introduced. (b) & (c) describe progression of flow from when the channel contains fresh water at $T=0$, to the introduction of salty liquid (c) at $T>0$ As time evolves to a large T , the blue color will eventually start to fade due to the action of diffusioosmosis and gravity.

4.1 Pure Diffusion

First, we considered the effect of having a flow strictly controlled by diffusion as the entire term of the first portion of the right-hand side of equation (46) is set to zero as expressed below:

$$\frac{\partial \overline{C}}{\partial T}=\ \mathcal{D}\varepsilon^2\frac{\partial^2\overline{C}}{\partial X^2}$$

We set $\mathcal{D} = 1$, and $\varepsilon = 0.1$ in a classic diffusion to see how the average concentration varies simultaneously with time and position along the channel. The curves in fig 7 show how the concertation of solution changes along the length of the channel whose flow is solely driven by diffusion or concentration gradients. Plots were generated from left to right, at $T1 =$ 1e-9 , $T2 = \ 0.025, T3 = \ 1.0, T4 = 10, and\ T5 = \ 40$. As time progresses, the concentration of the light solution increases whilst that of the denser solution decreases.

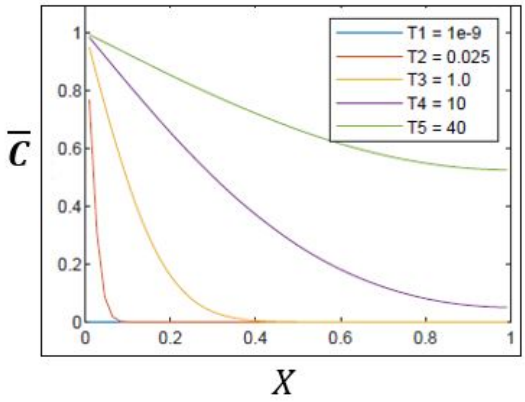

Figure 7. Pure Diffusion plot with average concentration ($\overline{\boldsymbol{C}}$) on the vertical axis and channel length (X) on the horizontal axis. Plot times are $1e-9$ (blue), 0.025 (red), 1.0 (yellow), 10 (purple), and 40 (green). $\mathcal{D} = 1,\ \varepsilon = 0.1$.

4.2 <u>The effect of gravity, with negligible impact of diffusioosmosis.</u>

We consider the effect of having a predominantly gravity-driven flow by turning off the entire second term of equation (46) $[\mathcal{D}\varepsilon^2 \frac{\partial \overline{C}}{\partial X}]$, and setting $D = 1,\ and\ \varepsilon = 0.1$. Although the diffusioosmosis and gravity terms in the same equation are coupled, we assume the long channel length renders the impact of diffusioosmosis in $\frac{4}{\mathcal{D}}\left(\frac{\partial \overline{C}}{\partial X}\right)^3 \frac{(27)}{2835}$ significantly less than the contribution from $\mathcal{D}\varepsilon^2 \frac{\partial \overline{C}}{\partial X}$ which was set to zero. The plots

obtained from figures 7 and 8 supports the claim that gravity plays a higher role, in that $T5$ plot terminates at a higher $\overline{C}$ here than the pure diffusion case where Γ was automatically zero. The axis and plot times are the same as the diffusion flow in section 4.1. We observed the impact of increasing the value Γ which implied changing the fluid properties. By reducing the viscosity, the influence of gravity also increases causing flow to proceed at a faster rate. So, at lower Γ values, the concentration profile for curves as time advances show slower progression when compared with higher values.

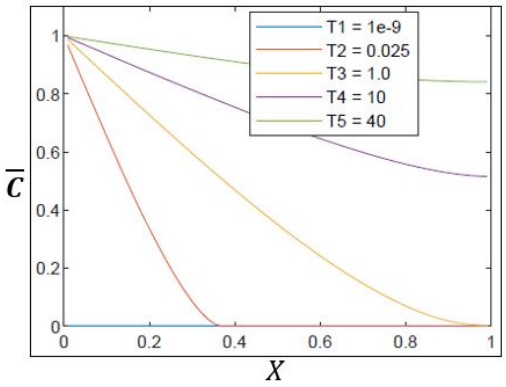

Figure 8. Plot of average concentration ($\overline{\boldsymbol{C}}$) vs channel length ($\boldsymbol{X}$) for Gravity-dominated flow channel, with some impact of diffusioosmosis. Plot times are $1e-9$ (blue), 0.025 (red), 1.0 (yellow), 10 (purple), and 40 (green). $\mathcal{D}=1$, $\varepsilon=0.1$, $\Gamma=5$.

4.3 The combined effect of diffusioosmosis and gravity – uncharged systems

Next, we consider the main situation of interest where both gravity and chemical potential influence the progression of flow thus favoring mixing. We will keep all parameters in equation 46 and adopt the same procedure including time plots used in section 4.2, increasing the value of Γ while keeping ε at 0.1, and accounting for slip conditions. As expected, the plot generated in figure 4.3 at $T=40$ terminated at slightly

higher average concentration than the previous case and much higher than the pure diffusion scenario. We also compared this result with Γ values of $1, 3, and\ 10$, and confirmed the flow increased while keeping ε and $\mathcal{D}$ constant. Comparing figure 9 with plots from figures 7 and 8, we noticed increase in flow due to the joint action of diffusioosmosis and gravity.

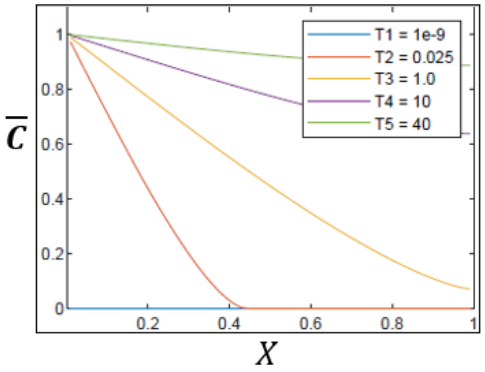

Figure 9. Plot of average concentration ($\overline{\boldsymbol{C}}$) vs channel length ($\boldsymbol{X}$) for Combined effect gravity and diffusioosmosis in **uncharged** systems. Plot times are $1e-9$ (blue), 0.025 (red), 1.0 (yellow), 10 (purple), and 40 (green). $\mathcal{D} = 1,\ \varepsilon = 0.1, \Gamma = 5$.

4.4 <u>The combined effect of diffusioosmosis and gravity – charged systems</u>.

When the fluid is charged the flow is faster than the uncharged fluid. Taking into consideration slip velocity condition at the top and bottom walls of the channel, we show this by choosing $\mathcal{D} = 1$, and $\Gamma = 5$. Unlike the in the previous cases, plots were generated at $T1 =$ 1e-9 , $T2 = 1e-7, T3 = 1e-5, T4 = 1e-3, and\ T5 = 0.025$. The last time plot was particularly chosen to serve as reference for comparison between the charged systems and the uncharged systems. We observed that in all cases previously considered, the channel is barely starting to get any flow at $T = 0.025$ whereas we saw a

rapid flow which caused the channel to fill up at the same T value. Starting from $\overline{\boldsymbol{C}} = 1$ at the channel inlet, the average concentration decreases as the effect of gravity increases and having the impact of diffusioosmosis.

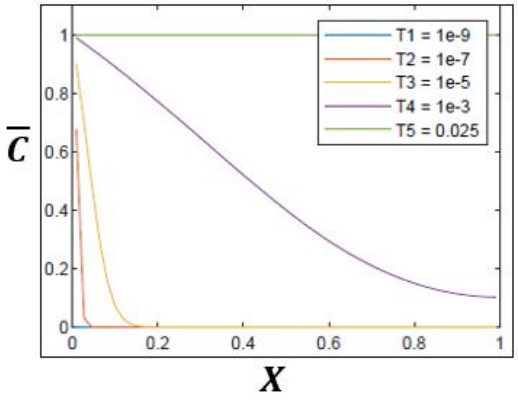

Figure 10. Plot of average concentration ($\overline{\boldsymbol{C}}$) vs channel length ($\boldsymbol{X}$) for Combined effect gravity and diffusioosmosis in **charged** systems. Plot times are $1e-9$ (blue), $1e-7$ (red), $1e-5$ (yellow), $1e-3$ (purple), and 0.025 (green). $\mathcal{D} = 1,\ \varepsilon = 0.1, \Gamma = 5$

We have seen how the average concentration $\overline{\boldsymbol{C}}$ varies in the channel as the solute moves from one position, $\boldsymbol{X}$ to another as time, T progresses. We have compared $\overline{\boldsymbol{C}}(\boldsymbol{X}, \boldsymbol{T})$ plots for pure diffusion, gravity effect and minimal diffusioosmosis, gravity effect with diffusioosmosis for both uncharged and charged systems. We observed from plots which channel fills up faster from the last average concentration gradient plots at time $T5$. It will be more beneficial from a product design precision standpoint to determine how long it would take to achieve a certain capacity of the average concentration.

4.5 Time to fill the channel.

Now, we seek to determine how long it will take for the average concentration in the channel to reach a certain target value, say 95% of the inlet concentration. We define another parameter mean concentration, $< C > (T)$ which is the average of the average concentration $\overline{\boldsymbol{C}}(X,T)$ eliminating the X dependence. That is, $< C > (T) = \int_0^1 \overline{C}(X,T)$.

We refer to tests performed in sections $8, 9, and\ 10$ keeping the values of $\mathcal{D}, \text{and } \varepsilon$ constant and changing Γ. First, we plot $< C > \text{vs } (T)$ with each plot representing different Γ values (we chose $\Gamma = 1, 2, 3, 5, 10$). The following plots (Figure $11(a) \text{through } 11(d)$) show how the mean concentration increases with time, as the value of Γ is raised. Plot $4.5(c) \text{ and } (d)$ represent the effect of both gravity and diffusioosmosis in charged systems, with (d) being an

expanded image for (c). As seen before, the flow is much faster in charged systems, filling the channel within a short amount of time. We observe that at around $T = 0.025$, we

attained 95 percent of the mean concentration, $< C >$, whereas the time was about 40 for combined diffusioosmosis with gravity in uncharged systems.

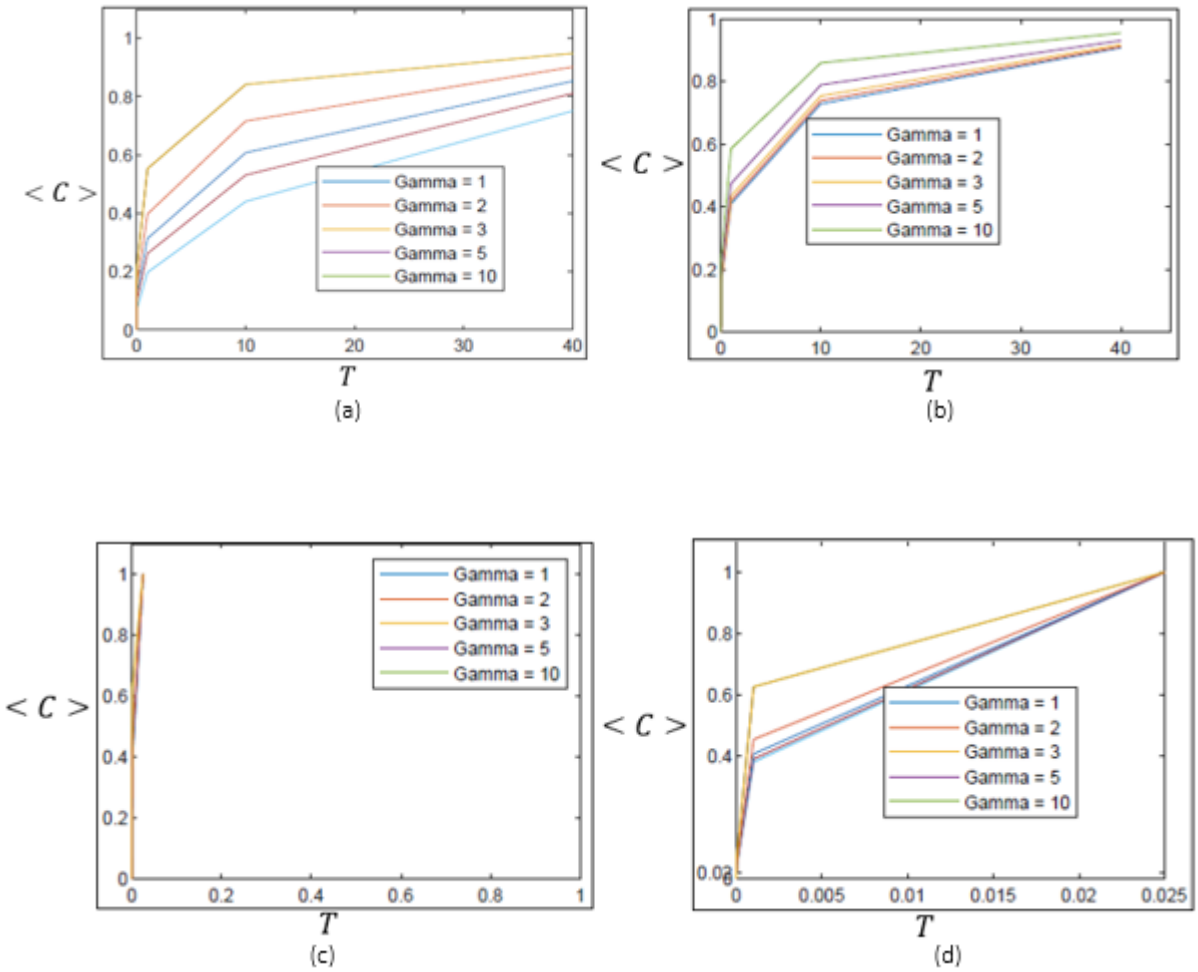

Figure 11. Plots of mean concentration, $< C > vs$ time, (T) .In plot (a), we have predominantly gravity enable flow with some diffusioosmosis. In plot (b), we have the combined effect of gravity and diffusioosmosis for uncharged systems. In plot (c), we have joint impact of diffusioosmosis and gravity for charged systems. $\mathcal{D} = 1,\ \varepsilon = 0.1, \Gamma = 1,2,3,5,10$.

The above plots give an idea in agreement with the previous section of which situations would be favorable for faster flow but, we still do not have a precise time at which we can reach any desired fraction of mean concentration. So, we extract the mean concentration values

generated from MATLAB simulations for each case in sections $8, 9, and\ 10$, but with five (5) values of Γ as shown in table 1 below.

Table 1. Mean concentration data generated from MATLAB for the effect of gravity and diffusioosmosis in charged system. $\mathcal{D} = 1,\ \varepsilon = 0.1, \Gamma = 1,2,3,5,10$.

	$< C >$				
T	**$\Gamma = 1$**	**$\Gamma = 2$**	**$\Gamma = 3$**	**$\Gamma = 5$**	**$\Gamma = 10$**
0	0.0001	0.0001	0.0001	0.0001	0.0001
1.04E-07	0.012779	0.012806	0.012851	0.012996	0.013674
1.00E-05	0.040388	0.041502	0.043295	0.048564	0.0675
0.001	0.380592	0.390759	0.407017	0.454457	0.625997
0.025	0.999316	0.999652	0.99989	0.999998	1

This is an example of data obtained for the charged system. We interpolation or extrapolation depending on where 95 percent (0.95) lies in the table. So, here we would have five (5) values of T_{95} . We repeat this process for other two cases to obtain two sets of five (5) T_{95} with the corresponding Γ values as shown in table 2.

Table 2. Calculated time to reach 95 percent of mean concentration. Data generated from MATLAB for the effect of gravity and diffusioosmosis in charged system. $\mathcal{D} = 1,\ \varepsilon = 0.1, \Gamma = 1,2,3,5,10.$

Γ	***Gravity only T_{95}***	***Gravity with Diffusioosmosis (Uncharged) T_{95}***	***Gravity with Diffusioosmosis (Charged) T_{95}***
1	*59.19175*	*47.28849*	*0.023087*
2	*54.93321*	*46.84411*	*0.023043*
3	*51.84218*	*46.17041*	*0.02298*
5	*47.7718*	*44.37925*	*0.0228*
10	*40.5098*	*38.79662*	*0.021791*

Next, we plot the T_{95} with the corresponding values of Γ in figure 12.

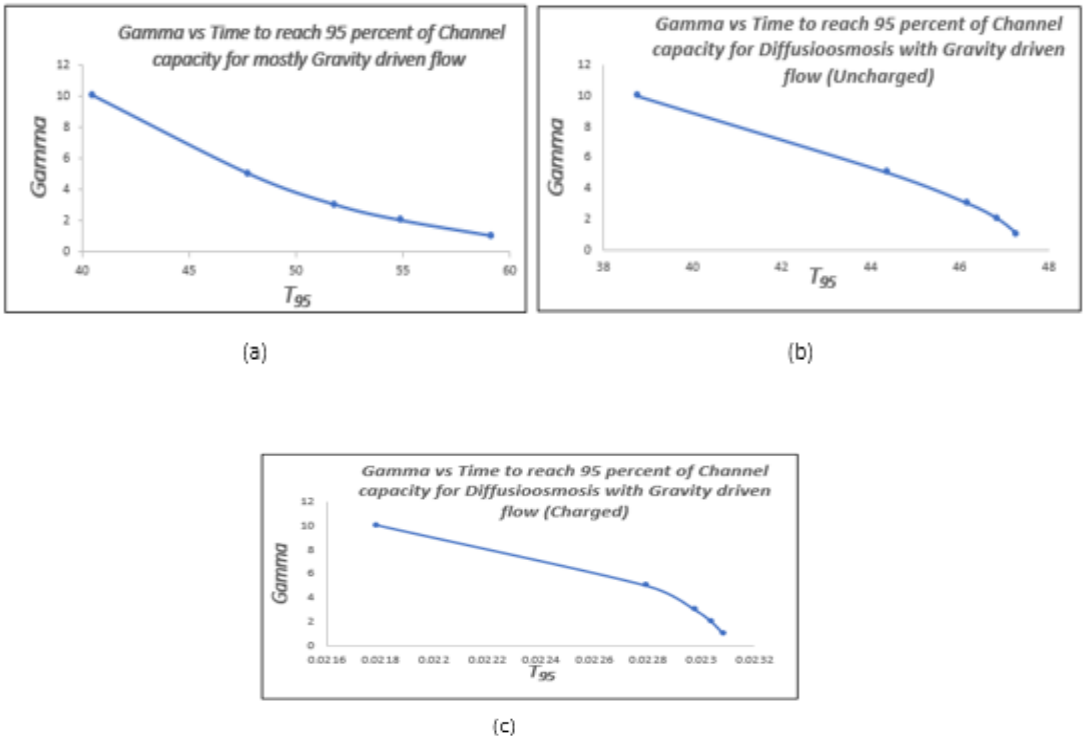

Figure 12. Plots of Gamma vs Time to reach 95 percent of average concentration, T_{95}. In plot (a), we have predominantly gravity enable flow with some diffusioosmosis. In plot (b), we have the combined effect of gravity and diffusioosmosis for uncharged systems. In plot (c), we have joint impact of diffusioosmosis and gravity for charged systems. $\mathcal{D} = 1,\ \varepsilon = 0.1, \Gamma = 1, 2, 3, 5, 10.$

Finally, we create a vector field plot for the effect of gravity and diffusioosmosis in uncharged system. We set $\mathcal{D} = 1,\ \varepsilon = 0.1, \Gamma = 10$, to obtain the velocity field in Fig. 13 showing a recirculating flow combined with slip at the walls.

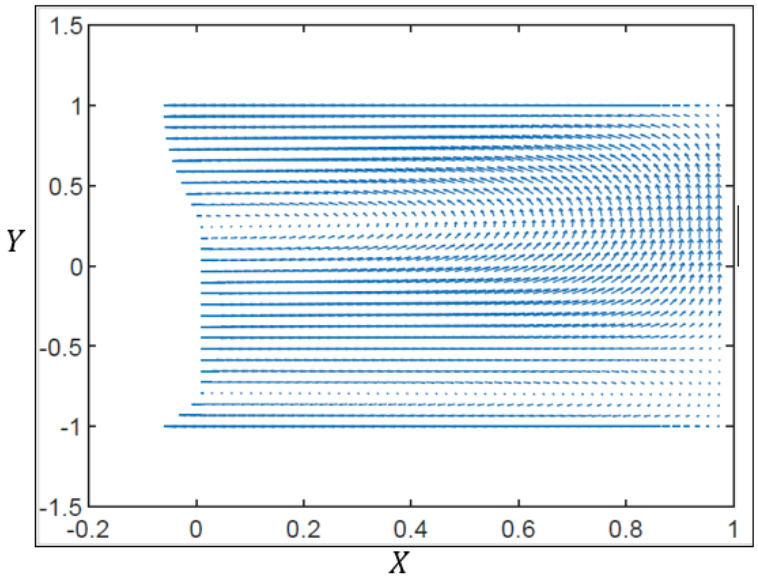

Figure 13. Vector field Plots of the combined effect of gravity and diffusioosmosis for uncharged systems at $T = 40$. We set the flow parameters for $\mathcal{D} = 1,\ \varepsilon = 0.1, \Gamma = 10$.

Chapter 5. CONCLUSIONS AND FUTURE WORK

We showed that, without external forces, gravity and chemical potential can drive flow concurrently. We formulated a problem involving the introduction of saltwater into a rectangular microfluidic channel containing fresh water. We focused on what happens as the dense salt solution contacts the less dense fresh water and the impacts on the resulting solution as time evolved. Starting with the Navier-Stokes equation and non-dimensionalizing, we obtained an expression for the horizontal velocity,$\boldsymbol{U}$ and substituted into the convection-diffusion equation, resulted in a complicated 2D coupled non-linear system. After applying averaging ideas following arguments of Taylor-dispersion, we derived an expression for concentration deviations, $\boldsymbol{C'}$ and, simplified the 2D system into a 1D non-linear system involving only the average concentration, $\overline{\boldsymbol{C}}$.

We performed mesh discretization using the finite Volume Method on the non-linear partial differential equation and completed the process with MATLAB simulations. We varied the fluid property, Γ for the effect of predominantly gravity with some diffusioosmosis, solely diffusioosmosis, and compared the outcomes with those obtained when both factors were jointly involved. The results show that flow proceeds faster with the joint action of gravity and diffusioosmosis, and even much faster when the system is charged.

There are possibilities for achieving further enhancement of solute transport by flow in future. Choosing a different orientation for the microfluidic channel such that it is

slightly slanted could enhance the effect of gravity since the results support that gravity plays a higher role in the mixing process. We could also decrease the length of the channel to allow for multiple mixing actions, smoothen the surfaces for easy charge dissipation, and use a cylindrical geometry channel. We could consider a multicomponent system such as a body fluid: the blood, containing plasma, red blood cells, white blood cells, and platelets, for drug delivery and therapeutic applications. Finally, careful upscaling of this work could be applied to various large scale industrial processes involving mixing.

REFERENCES

[1] Thomas, L.& Logan, J. Benefit of using a microfluidic device. News Medical Life Sciences. https://www.news-medical-.net/life-sciences/Benefits-of-a-microfluidic-Syatem.aspx.(2023)

[2] Huang, Y. & Streets, M. A. Chip in a lab: Microfluidics for next generation life science research. Biomicrofluidics. 7(1): 011302. doi:10.1063/1.4789751. (2013)

[3] Elve flow. 2023. Microfluidics: A general overview of microfluidics. https://www.elveflow.com/microfluidics-reviews/general-microfluidics/a-general-overview-of-microfluidics. (2023)

[4] Chiu, T.D., deMello, A.J., Carlo, D., Doyle, P., Hansen, C., Maceiczyk, R.M. & Wootton, R.C. Small but perfectly Formed? Successes, Challenges, and Opportunities for Microfluidics in the Chemical and Biological Sciences. Chem 2, 201-203. https://www.cell/chem/pdf/S2451-9294(17)30033-5.pdf .(2017)

[5] Zheng, G., Cui, Y., Lu, L., Guo, M., Hu, X., Wang, L., Yu, S., Sun, S., Li, Y., Zhang, X. & Wang, Y. Microfluidic chemostatic bioreactor for high-throughput screening and sustainable co-harvesting of biomass and biodiesel in microalgae. *Bioactive Materials.* Vol. 25, pages 629-639. https://doi.org/10.1016/j.bioactmat.2022.07.012.(2023)

[6] Zheng-Yi, L. & Xian, P. Application of Droplet-Based Microfluidics in Microbial Research. *PubMed*. *54*(3), 673–678. https://doi.org/10.12182/20230560303.(2023)

[7] Zhang, K., Qin, S., Wu, S., et al Microfluidic systems for rapid antibiotic susceptibility tests (ASTs) at the single-cell level. Chem Sci. 11(25):6352–6361. doi: 10.1039/d0sc01353f. (2020)

[8] Jiang, Y., Manz, A., Wu, W. Fully automatic integrated continuous-flow digital PCR device for absolute DNA quantification. *Anal Chim Acta*. 1125:50–56. doi: 10.1016/j.aca.2020.05.044. (2022)

[9] Whitesides, G. M. The origins and the future of microfluidics. *Nature*. 442(7101):368–373. doi: 10.1038/nature05058. (2006)

[10] Hengoju, S., Tovar, M., Man, D. K. W, et al. Droplet microfluidics for microbial biotechnology. *Adv Biochem Eng Biotechnol*.179:129–157. doi: 10.1007/10_2020_140. (2020)

[11] Precedence Research. Microfluidics Market- Global Market Size, Trends Analysis, Segment Forecasts, Regional Outlook 2023 – 2032. https://www.precedenceresearch.com/microfluidics-market

[12] Alessio, B.M., Shim, S., Gupta, A. & Stone, H.A. Diffusioosmosis-driven dispersion of colloids: a Taylor dispersion analysis with experimental validation. Journal of Fluid Mechanics. 942, A23. doi:10.1017/jfm.2022.321. (2022)

[13] Salmon, J., Soucasse, L., Doumenc, F. Role of solutal free convection on interdiffusion in a horizontal microfluidic channel. *Phys. Rev. Fluids* 6, 034501. (2021)

[14] Kreppenhofer, K., Li, J., Segura, R., Popp, L., Rossi, M., Tsvetkova, P., Luy, B., Kahler, C. J., Guber, A.E., & Levkin, P.A. Formation of a Polymer Surface with a Gradient of Pore Size Using a Microfluidic Chip. 3797-3804 Langmuir. dx.doi.org/10.1021/la304997a. (2013)

[15] Bastian E. Rapp. Microfluidics: Modeling, Mechanics, and Mathematics. 243 – 263, Micro and Nanotechnologies. https://doi.org/10.1016/B978-1-4557-3141-1.50009-5. (2017)

[16] Kamholz, A.E., Yager, P. Theoretical Analysis of Molecular Diffusion in Pressure-Driven Laminar Flow in Microfluidic Channels. Biophysical Journal 80(1) 155–160. (2001)

[17] Douglas P. Holmes. Confined Fluid Flow: Microfluidics and Capillarity. Boston University. https://www.bu.edu/moss/files/2015/08/Sapienza2015_Microfluidics.pdf

[18] Araz, M. K., Tentori, A.M., Herr, A.E. Microfluidics multiplexing in bioanalysis. National Library of Science. 18(5):350 – 66. doi: 10.1177/2211068213491408. (2013)

[19] Coulson, J., Richardson, J.F. Transport Processes in Microfluidic Applications. Coulson and Richardson's chemical engineering (Seventh edition). 2018, Pages 529-546. https://doi.org/10.1016/B978-0-08-102550-5.00006-7.

[20] Jesse T Ault, Sangwoo Shin, Howard A Stone. Characterization of surface-solute interactions by diffusioosmosis. *Soft Matter*. 15(7): 1582-1596. doi: 10.1039/c8sm01360h. (2019)

[21] Ian Williams, Sangyoon Lee, Azzurra Apriceno, Richard P Sear, Giuseppe Battaglia. Diffusioosmotic flows induced by a nonelectrolyte concentration gradient. Proc Natl Acad Sci *USA*.117(41):25263-25271. doi:10.1073/pnas.2009072117. (2020)

[22] Suin Shim. Diffusiophoesis, Diffusioosmosis, and Microfluidics: Surface-Flow-Driven Phenomena in the Presence of Flow. *Chem Rev*. 122(2):6986-7009. doi: 10.1021/acs.chemrev.1c00571. (2022)

[23] Wei-Shan Hsu, Anant Preet, Tung-Yi Lin, Tzu-En Lin. Miniaturized Salinity Gradient Energy Harvesting Devices. *Molecules*. 26(18):5469. doi: 10.3390/molecules26185469. (2021)

[24] Abecassis, B., Cottin-Bizonne, C., Ybert, C., Adjari, A. & Bocquet, L. Boosting migration of large particles by solute contrasts. *Nat. Mater*. 7 (10), 785-789. (2008)

[25] Abecassis, B., Cottin-Bizonne, C., Ybert, C., Adjari, A. & Bocquet, L. Osmotic manipulation of particles for microfluidic applications. *New J. Phys*. 11(7), 075022. (2009)

[26] Alessio, B.M., Shim, S., Mintah, E., Gupta, A. & Stone, H.A. Diffussiophoresis and diffusioosmosis in tandem: two-dimensional particle motion in the presence of multiple electrolytes. *Phys. Rev. Fluids* 6 (5), 054201. (2021)

[27] Banerjee, A., Williams, I., Azevedo, R.N., Helgeson, M.E. & Squires, T.M. Soluto-inertial phenomena: designing long-range, long-lasting, surface-specific interactions in suspensions. *Proc. Natl Acad. Sci.* 113 (31), 8612-8617. (2016)

[28] Biesheuvel, P. M. & Bazant, M.Z. Nonlinear dynamic of capacitive charging and desalination by porous electrodes. *Phys Rev.* E 81 (3), 031502. (2010)

[29] Aris, R. On the dispersion of a solute in a fluid flowing through a tube. Proc. R. Soc. Lond. Ser A. Math. Phys. Sci. 235 (1200), 67-77. (1956)

[30] Ault, J. T., Warren, P.B., Shin, S. & Stone, H. A. Diffusiophoresis in one-dimensional solute gradients. Soft Matt. 15, 1582-1596. (2017)

[31] Rubinstein, I. & Zaltzman, B. Convective diffusive mixing in concentration polarization: from Taylor dispersion to surface convection. J. Fluid Mech vol. 728. Pp. 239 – 278. doi:10.1017/jfm.2013.276. (2013)

[32] Kelley, W. J., Onyskiw, P.J., Fromen, C. A. & Eniola-Adefeso, O. Model Particulate Drug Carriers Modulate Leukocyte Adhesion in Human Blood Flow. ACS Biomater. Sci. Eng. 5, 6530-6540. doi: 10.1021/acsbiomaterials.9b01289. (2019)

[33] William, I., Lee, S., Apriceno, A., Sear, R. & Battaglia, G. 2020. Diffusioosmotic and convective flows induced by a nonelectrolyte concentration gradient. PNAS. 117(40), 25263-25271.www.pnas.org/cgi/doi/10.1073/pnas.2009072117. (2020)

[34] Huan J. Keh. Diffusiophoresis of charged particles and diffusioosmosis of electrolyte solutions. Current Opinion in Colloid & Interface Science. Elsevier. 24(2016) 13-22. http://dx.doi.org/10.1016/j.cocis.2016.05.008.

[35] Yakhshi-Tafti, E., Cho, H. J. & Kumar, R. Diffusive mixing through velocity profile variation in microchannels. Springler. Exp. Fluids. doi 10.1007/s00348-010-0954-5. (2010)

[36] Niazmand, H., Jamaati, J. & Farahinia, A. Investigation of slip effects on electroosmotic mixing in heterogeneous microchannels based on entropy index. SN Applied Sciences. https://doi.org/10.1007/s42452-019-0751-6. (2019)

[37] Kamholz, A.E., Yager, P., Weigl, B.H. & Finlayson, B.A. Quantitative Analysis of Molecular Interaction in a Microfluidic Channel: The T-Sensor. Anal. Chem. 71(23) 5340–5347. (1999)

[38] Perry, R.H. & Green, D.W, Eds., “Thermodynamics,” Chapter 4, in “Perry’s Chemical Engineers’ Handbook,” 7th ed., McGraw-Hill, New York (1984).

[39] Smith, J.M., Van Ness, H.C., Abbott, M.M. & Swihart, M.T. “The Framework of Solution Thermodynamics,” Chapter 10, in “Introduction to Chemical Engineering Thermodynamics,” 8th ed., (2017)

[40] Bird, R.B., Stewart, W.E.& Lightfoot, E.N. “Diffusivity and the Mechanisms of Mass Transport,” Chapter 17 in “Transport Phenomena,” Revised 2nd ed., (2007)